

TOWARD THE FORMATION OF CARBONACEOUS REFRACTORY MATTER IN HIGH TEMPERATURE HYDROCARBON-RICH ATMOSPHERES OF EXOPLANETS UPON MICROMETEOROID IMPACT

BENI B. DANGI¹, YONG S. KIM¹, SERGE A. KRASNOKUTSKI^{1,3}, RALF I. KAISER^{1,4}, AND CHARLES W. BAUSCHLICHER JR²

¹Department of Chemistry, University of Hawai'i at Manoa, Honolulu, HI 96822, USA

²Entry Systems and Technology Division, NASA Ames Research Center, Moffett Field, CA 94035, USA

Received 2014 November 18; accepted 2015 March 24; published 2015 May 21

ABSTRACT

We report on laboratory simulation experiments mimicking the chemical processing of model atmospheres of exoplanets containing C3 and C4 hydrocarbons at moderate temperatures of 400 K upon interaction of catalytic surfaces of micrometeoroids. By utilizing an ultrasonic levitator device and heating singly levitated particles under simulated microgravity conditions, Raman spectroscopy is utilized as a non-invasive tool to probe on line and in situ the conversion of C3 and C4 hydrocarbons to refractory carbonaceous matter on the surfaces of levitated particles. Secondary Ion Mass Spectrometry and electron microscopic imaging were also conducted to gain further insight into the elementary composition and structures of the refractories formed. Our results provide compelling evidence that in the presence of a catalytic surface, which can be supplied in the form of micrometeoroids and atmospheric dust particles, hydrocarbon gases present in the atmospheres of exoplanets can be converted to refractory, carbon-rich carbonaceous matter of mainly graphitic structure with a carbon content of at least 90% at elevated temperatures. This finding might explain the low methane to carbon monoxide (CH₄–CO) ratio in the hot Neptune GJ 436b, where the abundant methane photochemically converts to higher order hydrocarbons and ultimately to refractory graphite-like carbon in the presence of a silicon surface.

Key words: astrochemistry – planets and satellites: atmospheres – solid state: refractory – techniques: imaging spectroscopy

1. INTRODUCTION

Among 1767 confirmed exoplanets as of 2014 October, the vast majority hold atmospheric temperatures between 200 and 2000 K with sizes from 1 to 10 times the Earth (2014a). Although the bulk compositions of these exoplanets and the chemical makeup of their atmospheres are largely unknown, with the help of astronomical observations coupled with atmospheric modeling, an understanding of the chemical evolution of the hydrocarbon-rich atmospheres of exoplanets, mainly of hot Jupiters (HD 209458b, HD 189733b; Moses et al. 2011) and hot Neptunes (GJ 436b; Yurchenko et al. 2014), is slowly beginning to emerge. Features at about 3.25 μm are interpreted in terms of non-local equilibrium emissions from methane (CH₄; Janson et al. 2013). Methane has also been directly imaged in the cooler atmosphere of GJ 504 b at about 510 K (Janson et al. 2013) and in the atmosphere of the super-Earth GJ 1214b (Kreidberg et al. 2014). In these atmospheres, Ly α radiation from the host star of the exoplanet initiates a rich photochemistry at temperatures as high as a few 1000 K (Schindhelm et al. 2012). This photochemistry has been attributed to the lack of methane, for instance in GJ 436b, implying that methane might be converted into spectroscopically non-detectable carbonaceous matter—possibly of refractory nature—even at atmospheric temperatures as low as 500 K. Stevenson et al. verified that methane photochemistry and polymerization of methane into C2 to C4 hydrocarbons are required to explain the low methane (CH₄) to carbon monoxide (CO) ratio of the hot Neptune GJ 436b, which is a factor of about 100 smaller than predicted

(Stevenson et al. 2010). Rimmer et al. (2014) proposed that even galactic cosmic-ray processing of atmospheres of free-floating exoplanets without significant Ly α exposure might be linked to the formation of complex C2 to C4 hydrocarbons from methane, eventually leading to haze as observed in upper atmospheres of various exoplanets such as of GJ 1214b (Bean et al. 2010; Wilson et al. 2014) and HD 189733b (de Kok et al. 2013).

To interpret the hitherto unresolved lower-than-expected-abundance or even lack of atmospheric methane, sophisticated photochemical models of methane-rich atmospheres of exoplanets simulating the chemical evolution of carbonaceous matter at temperatures up to 1000 K have been developed exploiting Monte-Carlo transport models (Line et al. 2011; Venot et al. 2012; Morley et al. 2013). Initiated via Ly α photolysis, methane decomposes to the methyl radical (CH₃) plus atomic hydrogen with internally (rovibrationally) excited methyl radicals fragmenting to carbene (CH₂) and/or methyldiyne (CH) plus atomic/molecular hydrogen. These fragments either react with each other or with a second methane molecule leading to C2 hydrocarbons acetylene (C₂H₂), ethylene (C₂H₄), and ethane (C₂H₆; Line et al. 2011). Photodissociation of the latter and successive reaction of the fragments with C1 and C2 hydrocarbons lead to the synthesis of even heavier hydrocarbons such as C3 (methylacetylene, allene, propane) and C4 (1,3-butadiene, butane, butene). In the presence of nucleating particles such as micrometeoroids and dust particles with sizes ranging from a few millimeters to some 10 μm , (Mena et al. 2010; Adibekyan et al. 2012) more complex carbonaceous compounds of hitherto unknown chemical composition can form as deposits on these particles such as those evident from the dark Axel–Danielson dust and the bluish haze layer of the hot Jupiter HD 189733b (Mousis et al. 2011). Detailed mechanisms leading from small (C1 to C4)

³ Visiting Scientist; permanent address: Laboratory Astrophysics Group of the Max Planck Institute for Astronomy at the Friedrich Schiller University Jena, Helmoltzweg 3, D-07742 Jena, Germany.

⁴ Author to whom all correspondence should be addressed.

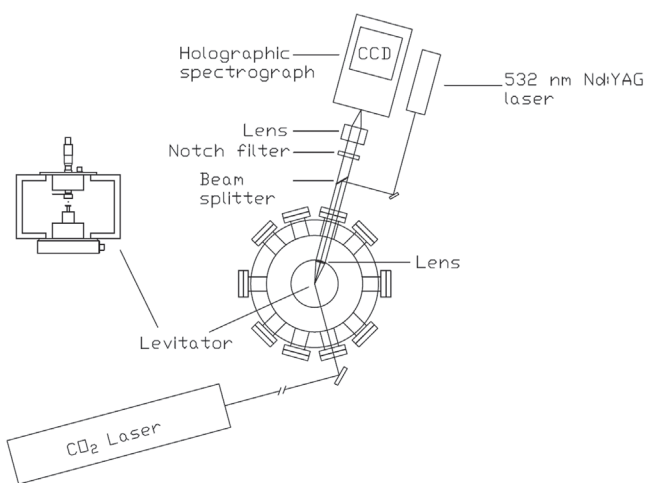


Figure 1. Schematic top view of the experimental setup. The levitator apparatus is situated at the center of the process chamber. The second copper mirror is not shown for clarity.

hydrocarbons, which are predicted in significant abundances as non-equilibrium species in the lower atmosphere of, for instance, the hot Neptune GJ 436b (Line et al. 2011), to (polymeric) carbonaceous matter are largely unknown, but have been proposed to involve polycyclic aromatic hydrocarbons (PAHs) and soot-like particles in the presence of catalytic surfaces at elevated temperatures (Cadwell et al. 1994). However, as of today, no laboratory experiments simulating the transformation from simple C1 to C4 hydrocarbons to carbonaceous refractories in hydrocarbon-rich atmospheres of exoplanets at elevated temperatures in the presence of catalytic surfaces have been reported in the literature.

Here, we report on laboratory simulation experiments mimicking the chemical processing of model atmospheres of exoplanets containing C3 and C4 hydrocarbons at moderate temperatures of 400 K upon interaction with catalytic surfaces of micrometeorites. By utilizing an ultrasonic levitator device and heating singly levitated particles under simulated micro-gravity conditions, Raman spectroscopy (Sadezky et al. 2005; Brunetto et al. 2009) is utilized as a non-invasive tool to probe on line and in situ the conversion of C3 to C4 hydrocarbons to refractory carbonaceous matter on the surfaces of these levitated particles. Secondary Ion Mass Spectrometry (SIMS) and electron microscopic imaging were also conducted to gain further insight into the elementary composition and structures of the refractories formed. Our studies demonstrate, for the very first time, that the synthesis of carbonaceous refractory matter with carbon content greater than 90% from C3 to C4 hydrocarbons in simulated hydrocarbon-rich atmospheres of exoplanets upon heating the catalytic grain surfaces to 400 K is facile, eventually leading to the formation of graphite-like carbonaceous matter.

2. EXPERIMENTAL AND THEORETICAL METHODS

Single silicon grains (99.9995%; Alpha Aesar) of 1 mm in diameter are levitated inside an ultrasonic levitator under container-less conditions. Briefly, the levitation device is based on a modified Tec5 AG-type acoustic levitator, which is housed within a 20 liter stainless steel process chamber (Figure 1; Brotton & Kaiser 2013a, 2013b). A standing ultrasound wave

is generated by a piezoelectric transducer, which oscillates at 58 kHz, via multiple reflections of the sound waves between the transducer and the concave-shaped reflector. Considering the acoustic radiation pressure and the counteracting gravitational force, the silicon grain is levitated slightly below the pressure minima of the standing wave (Xie & Wei 2001). A MagiDrive rotary micrometer manipulator is connected to the reflector and allows the distance between the transducer plate and the reflector to be adjusted from outside the process chamber to an integral number of half wavelengths so that the resonance condition can be maintained following changes in the ambient gas density, composition, temperature, and pressure. Owing to the curved reflector, the standing wave is not entirely planar, but slightly concave. The transverse component produces a radial restoring force, which centers the particle on the axis of the levitator, preventing the particle from drifting away.

The silicon grains were placed onto an acoustically transparent wire mesh with 88% surface opening, and the process chamber was evacuated by oil-free pumps to a pressure of typically 10^{-7} Torr. The chamber was then filled with the mixture of a process gas (100 Torr) and nitrogen at 293 K to a total pressure of 700 Torr. Separate experiments were conducted with the following process gases with the supplier and purity indicated in parentheses: methylacetylene (CH_3CCH ; 99+%; Organic Technologies), allene (H_2CCCH_2 ; 99+%; Organic Technologies), 1,2-butadiene ($\text{H}_2\text{CCCH}(\text{CH}_3)$; 98+%; Chem-Samp Co), 1,3-butadiene ($\text{C}_2\text{H}_3\text{C}_2\text{H}_3$; 99+%; Aldrich), and 2-butyne (CH_3CCCH_3 ; 99+%; Aldrich). Ultrasonic sound waves were generated by the piezoelectric transducer with a wavelength (λ) of $\lambda = 5.9 \pm 1.0$ mm. A linear transfer mechanism, which was interfaced to the acoustically transparent wire mesh, was moved toward the pressure node resulting in the levitation of a single particle. To heat the levitated particle, we exploited a 40 W carbon dioxide laser ($10.6 \mu\text{m}$; Synrad, Inc.). In the present experiments, only low power (1–3 W) was exploited to heat the levitated particle; for this, a planar copper mirror and a zinc selenide (ZnSe) window interfaced to the process chamber are employed to introduce the infrared (IR) beam (10 mm diameter at the levitation axis) to the levitated particle. Since the levitated particle rotates continuously during the irradiation, these conditions create a homogeneous heating of the particle. Furthermore, a second copper mirror installed within the process chamber behind the center of the levitator reflected the IR beam, resulting in homogeneous heating and increased stability of the levitated grain.

To monitor the chemical modifications of the levitated particles, Raman spectra were recorded on line and in situ (Brotton & Kaiser 2013a, 2013b). A Q-switched Nd:YAG laser (Crystalaser: QG-532-1W) was operated at 532 nm, repetition rate of 500 Hz, output power of 200 mW, and pulse width of 13.5 ns. The beam—exiting with a diameter of 0.35 mm and a divergence of 3.8 mrad—was split by a dichroic beam splitter, which reflected the laser beam toward the levitated sample, but also transmitted the Raman-scattered wavelengths. The average temperature at the gas-surface interface is estimated 400 K. A 532 nm notch holographic filter prevented the 532 nm Rayleigh scattering from reaching and damaging the CCD camera. The Raman-scattered light was focused by a Nikon 50 mm f/1.8 D-AF camera lens through a slit into a HoloSpec f/1.8 holographic imaging spectrograph. The slit width of $100 \mu\text{m}$ yielded a wavenumber resolution of 9 cm^{-1} . After passing through the slit,

the diverging beam was collimated by a lens toward two holographic transmission gratings (Princeton Instruments). One grating dispersed the low Raman shift wavenumbers from 168 to 2388 cm^{-1} , whereas the second separated the higher Raman shifts in the $2265\text{--}4387\text{ cm}^{-1}$ range. The thermoelectrically cooled CCD camera contained 1024×256 pixels. The final spectra for each spectral range were obtained by summing the total counts recorded in each pixel perpendicular to the dispersion axis simultaneously covering both spectral ranges as defined above. The Raman shifts were calibrated using cyclohexane (C_6H_{12}). This pulsed laser setup and the gated detector present a crucial prerequisite to reduce the fluorescent background. By varying the delay between the laser pulse and opening the gate to collect the CCD signal (gate delay) and also the gate opening (period), it is feasible to detect the faster Raman signal while discriminating from the longer-lived fluorescence. For the present experiments, typical values for the gate delay and period were optimized to 490 and 45 ns, respectively, with respect to the time zero trigger sent simultaneously to the laser and CCD gate.

The processed grain was removed from the chamber and further analyzed by micro-Raman spectroscopy with continuous 785 and 514 nm excitation. For the 785 nm excitation, the grain was placed on polished aluminum slide under microscope and excitation laser (Invictus). The excitation light was focused to an $8\text{ }\mu\text{m}$ spot. Spectra were excited with 3 mW of laser power on the sample and recorded in the spectral range of $4000\text{--}200\text{ cm}^{-1}$ (RXN system, Kaiser optical Systems Inc.). Each spectrum was collected for 20 s integration time and averaged for 10 measurements. Cosmic rays were removed from the spectra by utilizing a built-in software function. The measured spot on the grain was noted by taking an image and regained for 514 nm excitation in another micro-Raman spectrometer. Spectra were also taken at various spots on the grain to check uniformity of the carbon deposition. An argon laser (Ion laser technology 5500) was used for the 514 nm excitation with 2 mW laser power. Raman spectrum was recorded for 100 s excitation in the $4000\text{--}200\text{ cm}^{-1}$ (Renishaw system) range with cosmic-ray correction. Finally, the processed grains were analyzed utilizing SIMS to determine the carbon-to-hydrogen ratio of the deposited material on the silicon grain (Evans Analytical Group 2014b). Imaging of the processed samples were carried out by utilizing scanning electron microscopy (SEM; Hitachi S-4800 FESEM) and transmission electron microscopy (TEM; Hitachi HT7700).

For the computations, we exploited Density Functional Theory (DFT) to predict the Raman intensities for $\text{C}_{96}\text{H}_{24}$, $\text{C}_{150}\text{H}_{30}$, $\text{C}_{216}\text{H}_{36}$, $\text{C}_{294}\text{H}_{42}$, and $\text{C}_{384}\text{H}_{48}$. The B3LYP hybrid functional (Becke 1993; Stephens et al. 1994) was used in conjunction with the 4-31G basis set (Frisch et al. 1984). These molecules, which are part of the circumcoronene family of PAHs, have been studied previously (Ricca et al. 2012) at the same level of theory. In an earlier work, the harmonic frequencies and IR intensities were reported. In this work, we recompute the harmonic frequencies, but now also determine the Raman intensities. A comparison of the Raman intensities for $\text{C}_{96}\text{H}_{24}$ computed using the BP86 functional (Perdew 1986; Becke 1988) show that the choice functional does not strongly influence the results; for example, the maximum difference between in the intensities computed using the two functionals is less than 3% for any of the bands that account for more than 5% of the total Raman intensity. The DFT calculations were

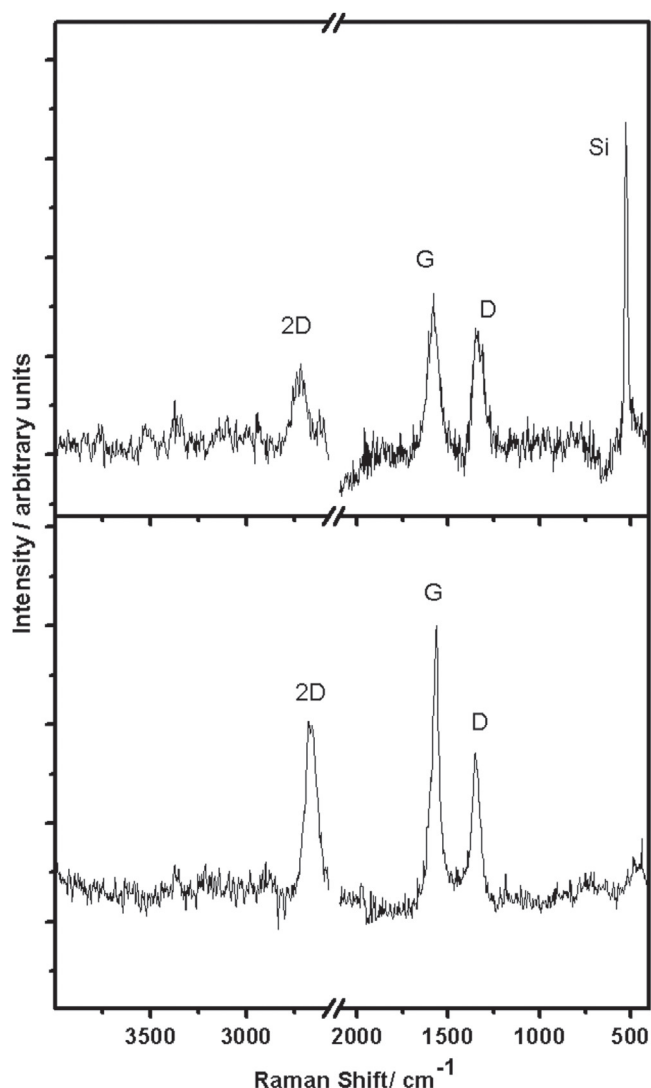


Figure 2. In situ Raman spectra of the processed silicon grain in methylacetylene gas (top) and of a levitated graphite grain in nitrogen (bottom).

performed using Gaussian09 (Frisch et al. 2013). The interactive molecular graphics tool MOLEKEL (Portmann & Luthi 2000) was used for the visualization of the molecular structures and the vibrational modes.

3. RESULTS

As evident from the in situ Raman spectrum of a processed silicon grain in methylacetylene gas, multiple new features emerged (Figure 2). Aside from the silicon band at 520 cm^{-1} , the Raman spectrum depicts three pronounced bands at 1350, 1580, and 2700 cm^{-1} . None of these bands were observed in control experiments without the silicon grain, implying that the new features arise from surface catalysis. The band at 1350 cm^{-1} is characteristic of the ring-breathing modes of sp^2 carbon atoms or defect band (D band) in polycrystalline graphite (Ferrari 2007). As documented by Ferrari (2007) the band at 1580 cm^{-1} is connected with the in-plane vibrational mode of graphite (G band) with the band around 2700 cm^{-1} originating from the D-band overtone vibration (2D band) of graphite. A comparison of the processed sample with the

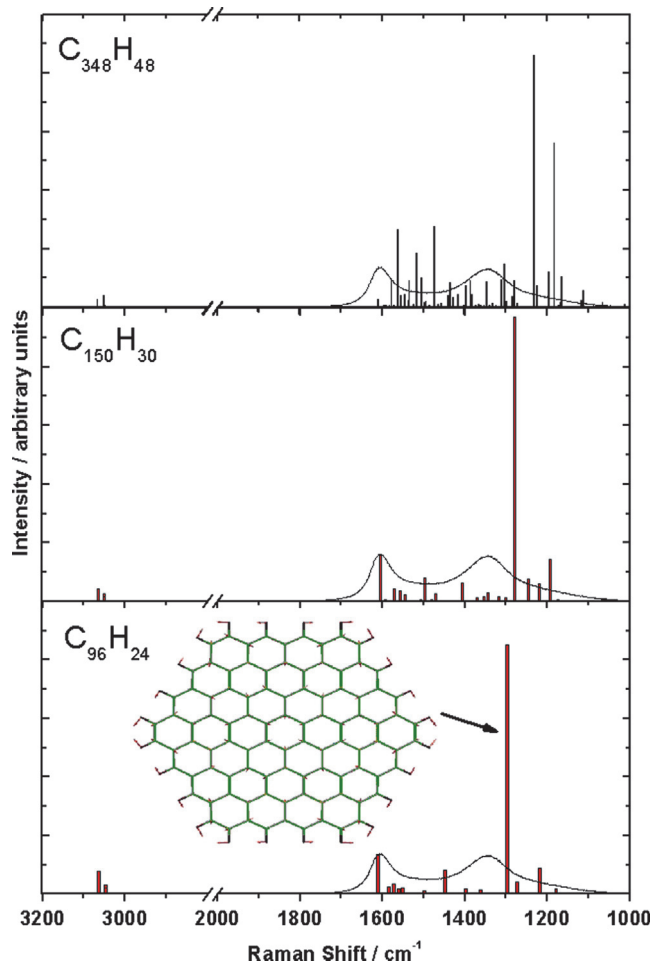


Figure 3. Calculated Raman spectra (bars) compared to the experimental spectra (curves) for three free polycyclic aromatic hydrocarbons; $C_{348}H_{48}$, $C_{150}H_{30}$ and $C_{96}H_{24}$. The vibrational mode responsible for the most intense calculated peak in $C_{96}H_{24}$ is also shown. Intensities are scaled to best match the calculated and experimental spectra.

Raman reference spectra of polycrystalline graphite recorded in the same levitator (Figure 2) and from the literature (Origlieri 2014) indicates that the processed sample contains carbon-rich graphite-like depositions. The in situ Raman measurements of the deposition process yielded growth spectra with saturation typically obtained after 3 hr of irradiation time. The diminished intensity of the 2D band compared to the D feature and the absence of the radial breathing mode around 250 cm^{-1} suggests a formation of carbon-rich PAH-like structures (Negri et al. 2002; Dresselhaus et al. 2005).

In an attempt to gain further insight into the nature of the newly formed deposits, we attempted to compare calculated Raman spectra of several carbon-rich PAHs with experimental spectra as shown in Figure 3. Spectra were calculated for $C_{348}H_{48}$, $C_{150}H_{30}$, and $C_{96}H_{24}$. Note that due to relatively small abundance in high frequency region, experimental spectra are not shown for that region. These comparisons depict that spectra can be qualitatively matched except for a strong band at around $1200\text{--}1300\text{ cm}^{-1}$; the latter arises from the vibration of terminal C–H groups. Therefore, we propose that the carbonaceous matter deposited is carbon rich and contains PAH- and graphitic-like carbon hexagon structures, but with a lower hydrogen content compared to the computed PAHs. We further analyzed the experimental spectra by deconvoluting the

Raman spectrum covering the region of the D and G bands ($2000\text{--}1000\text{ cm}^{-1}$; Figure 4 center panel). The spectrum can be fit with the combination of five Gaussian peaks centered at 1604 , 1515 , 1348 , 1234 , and 1100 cm^{-1} with FWHM of 60 , 230 , 111 , 168 , and 123 cm^{-1} , respectively. The overall shape of the spectra of all processed samples is matched very well with PAH-rich soot spectra (Sadezky et al. 2005; Brunetto et al. 2009). The 1604 cm^{-1} band is attributed to the graphitic G band (E_{2g}) with the broad feature at 1515 cm^{-1} originating from sp^2 amorphous carbon. The 1348 cm^{-1} band is also present in graphite and is characteristic of graphite layer edges (A_{1g}); the 1234 and 1100 cm^{-1} bands originate from disordered graphitic lattice. The bottom panel of Figure 4 shows the enhanced spectra in higher and lower frequency ranges. In the high frequency region, the peak near 2930 cm^{-1} with FWHM of 34 cm^{-1} can be attributed to the C–H stretching vibration while a broader peak near 827 cm^{-1} with FWHM of 62 cm^{-1} is likely due to the transverse optic (TO) phonon feature in Si–C vibration (Wieligor et al. 2005). This presents compelling evidence that the silicon surface is actively engaged in the chemistry of the formation of the carbonaceous matter. In short, the enhanced intensity of the D band compared to the 2D feature and C–H vibrational mode likely indicates the presence of hydrogen-deficient PAH- and soot-like material (Negri et al. 2002). Thus, we propose that the deposits do not only contain carbon, but also to a lesser extent hydrogen. In order to quantify the carbon-to-hydrogen ratios in the samples, the processed samples were analyzed by exploiting SIMS. These studies suggest that the samples are carbon-rich ($90\% \pm 5\%$) with only smaller fractions of hydrogen ($10\% \pm 5\%$). This carbon-to-hydrogen ratio was found to be invariant with the depth of the deposition down to about $300 \pm 10\text{ nm}$. It is important to highlight that the Raman spectrum of the processed sample is effectively invariant on the nature of the C3 and C4 hydrocarbons exploited in the experiments (Figure 4, top panel).

Finally, we characterized the processed samples via SEM (Figures 5(a) and (b)) and TEM (Figure 5(c)). In general, these images confirm the formation of carbonaceous deposits, as indicated by the Raman spectroscopy. Furthermore, the SEM images depict that the deposits are formed in fairly uniform shapes and sizes representing dome-like structures of about $1\text{ }\mu\text{m}$ in diameter. Similar structures were reported previously to be formed by exposing liquid benzene (Simakin et al. 2000) and toluene (Shafeev et al. 1999) on silicon surfaces to 510.6 nm radiation. A closer look at Figure 5(b) proposes the existence of smaller substructures, which cannot be further characterized due to the resolution limit of the SEM. Therefore, TEM images were taken of the deposit. These images expose needle-like substructures with diameters of less than typically 10 nm and facets likely due to the graphitic structures. No indication of tube structures is evident which supports the Raman analysis of the deposit.

4. ASTROPHYSICAL IMPLICATIONS AND CONCLUSIONS

Having exposed a novel formation path to form carbonaceous, graphitic matter at elevated temperatures on singly levitated particles, we are now discussing the implications of these results for exoplanetary environments. Our results provide compelling evidence that in the presence of a catalytic surface, which can be supplied in the form of micrometeoroids

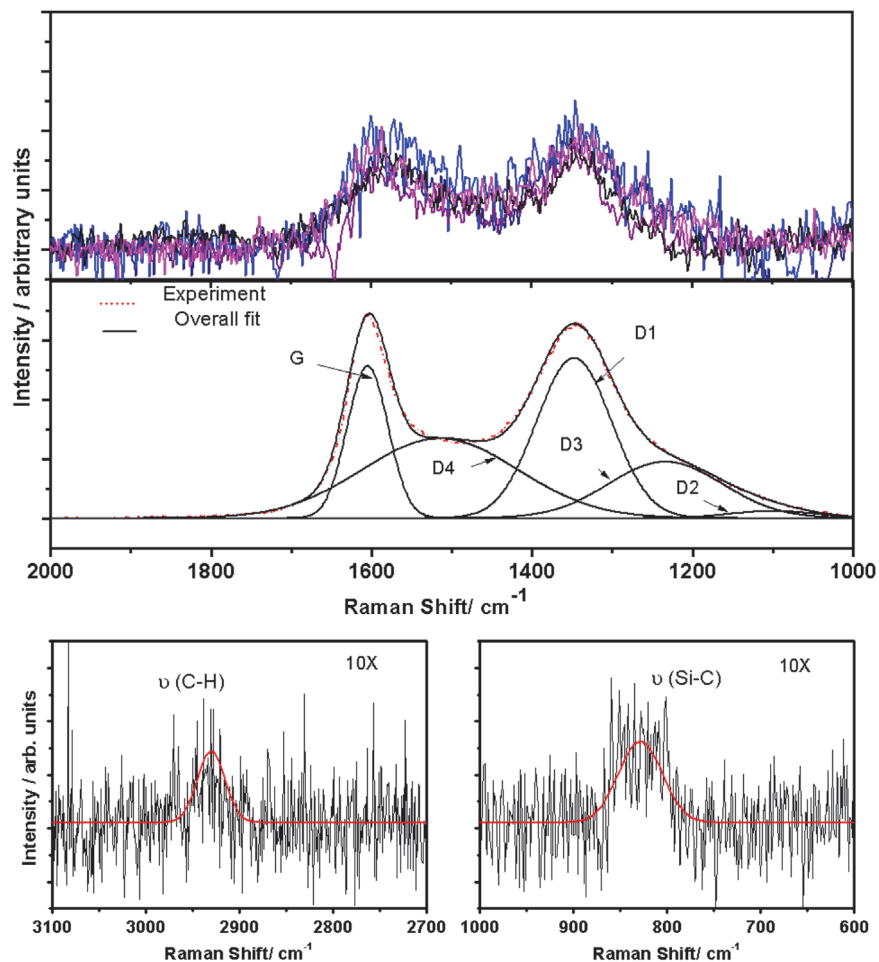


Figure 4. In situ Raman spectra of processed silicon grains in methylacetylene (magenta), allene (navy), 1,2-butadiene (blue), 2-butyne (black), and 1,3-butadiene (purple) in the top panel. The center panel shows the deconvoluted G and D bands along with the micro-Raman spectra of offline processed grains. Magnified micro-Raman spectra at higher and lower range are shown in the bottom panel.

and atmospheric dust particles, hydrocarbon gases present in the atmospheres of exoplanets can convert to refractory, carbon-rich carbonaceous matter with a carbon content of at least 90% at elevated temperatures. This finding might explain the low methane to carbon monoxide (CH_4 -CO) ratio in the hot Neptune GJ 436b, where the abundant methane photochemically converts to higher C2 to C4 hydrocarbons and hence ultimately to refractory carbon. These results also suggest that the dark Axel-Danielson dust and possibly the bluish haze layer of the hot Jupiter HD 189733b (Mousis et al. 2011) may contain complex carbonaceous matter as micrometer-sized particles form easily under the host star's irradiation. The results presented here should further trigger more detailed laboratory and modeling studies to understand the chemical evolution of hydrocarbon-rich atmospheres of exoplanets mainly of hot Jupiters (HD 209458b, HD 189733b; Moses et al. 2011) and of hot Neptunes (GJ 436b; Yurchenko et al. 2014), in particular in the presence of catalytic dust grains and/or micrometeoroids.

Note that strong IR emission bands between 3.3 and 13.5 μm were observed by the Kuiper Airborne Observatory in the carbon-rich planetary nebulae NGC 7027 (Russel et al. 1977) and HD 44179 (Russel et al. 1978). These bands are, in general, believed to be carried by carbon-based material, which by comparison with the laboratory experiments have been

assigned C-H and C-C stretching as well as bending modes likely due to a complex mixture of complex hydrocarbon structures such as alkenes, cyclic alkanes, and PAHs (Duley & Williams 1981). Our results imply that the complex refractory mixture of carbonaceous compounds can potentially form and accrue in gas-surface interactions during the evolutionary phase of planetary nebulae since various C2 to C6 hydrocarbon molecules such as benzene have been detected in protoplanetary nebula such as AFGL 618 (Cernicharo et al. 2001; Pwa et al. 1986). However, the validity of extrapolating our laboratory experiments to planetary nebulae remains to be tested in future simulation experiments as the effect of the gas pressure on the structure of the refractories deposited on the grain surface has not been investigated yet.

Finally, we would like to discuss the potential limitations and difficulties of our experimental approach. Recall that the present work represents the very first step toward an understanding of the conversion of hydrocarbons in the atmospheres of hot Jupiters and hot Neptunes in the presence of catalytic surfaces. The temperature and pressure in our study mimic the physical conditions in the atmospheres of exoplanets. These studies can be expanded systematically in the future to probe cumulative effects on the growth of graphite-like refractories by heating the levitated particle and simultaneous ultraviolet (UV) irradiation. In these future experiments, homogeneous

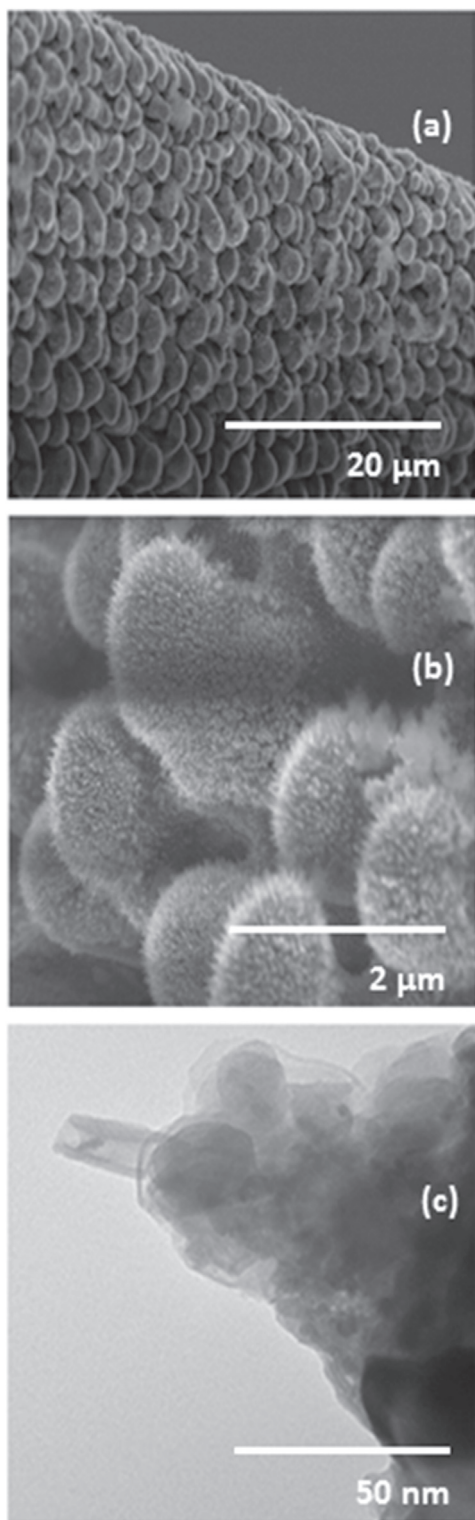


Figure 5. Surface imaging of the processed samples exploiting ((a) and (b)) scanning electron microscopy (SEM) (c) and transmission electron microscopy (TEM).

heating by carbon dioxide laser will simulate the actual temperature of the atmosphere of the exoplanet, whereas the UV exposure will mimic the radiation field from the central star. By exploiting monochromatic UV light, this might even yield information on the wavelength-dependent deposition of graphitic refractory materials on the surface of levitated

particles. This might also yield valuable information on the underlying—hitherto unknown—reaction mechanism. Based on the detection of the silicon–carbon stretching mode, an active chemistry of the catalytic surface might be postulated. Further, the laboratory studies were conducted with pure silicon grains as a proof-of-concept study by starting with chemically simple grains and demonstrating that based on the silicon–carbon (Si–C) bond formation, an active surface chemistry is ongoing and required. Future experiments will also probe silicates, silicon oxides, and silicon carbide grains to gain a more systematic understanding of how the substrate influences the chemical composition of the refractories formed. However, it should be stressed that a solid surface is required to form carbonaceous refractory material. Blank experiments conducted without the levitated particles and by solely heating the gas mixture with the carbon dioxide laser at identical power do not form any refractory materials, thus underlining the surface-mediated chemistry. Finally, future experiments will probe a systematic dependence of the formation of the refractories as a function of various gases on the chemicals (C1 to C4 hydrocarbons); current photochemical models propose that C1 hydrocarbons can be first converted to higher C2 to C4 hydrocarbons.

The authors thank Tina Carvalho of the University of Hawaii Biological Electron Microscope Facility for help with the SEM and TEM image acquisition. Funding for the research from the National Science Foundation (CHE-1360658) is greatly acknowledged. They would also would like to thank Dr. Anupam Mishra and Tayro Acosta of the Hawaiian Institute of Geophysics and Planetology (HIGP) for the use of micro-Raman systems and Professor Yuk L. Yung (California Institute of Technology) for helpful discussions.

REFERENCES

- 2014a, <http://exoplanetarchive.ipac.caltech.edu/index.html>
 2014b, <http://www.eag.com/mc/secondary-ion-mass-spectrometry.html>
 Adibekyan, V. Z., Santos, N. C., Sousa, S. G., et al. 2012, *A&A*, 543, A89
 Bean, J. L., Kempton, E. M. R., & Homeier, D. 2010, *Natur*, 468, 669
 Becke, A. D. 1988, *PhRvA*, 38, 3098
 Becke, A. D. 1993, *JCP*, 98, 5648
 Brotton, S. J., & Kaiser, R. I. 2013a, *JPCL*, 4, 669
 Brotton, S. J., & Kaiser, R. I. 2013b, *RSI*, 84, 055114
 Brunetto, R., Pino, T., Dartois, E., et al. 2009, *Icar*, 200, 323
 Cadwell, B. J., Wang, H., Feigelson, E. D., & Frenklach, M. 1994, *ApJ*, 429, 285
 Cernicharo, J., Heras, A. M., Tielens, A. G. G. M., et al. 2001, *ApJL*, 546, L123
 de Kok, R. J., Brogi, M., Snellen, I. A. G., et al. 2013, *A&A*, 554, A82
 Dresselhaus, M. S., Dresselhaus, G., Saito, R., & Jorio, A. 2005, *Phys. Rep.-Phys. Lett.*, 409, 47
 Duley, W. W., & Williams, D. A. 1981, *MNRAS*, 196, 269
 Ferrari, A. C. 2007, *SSCom*, 143, 47
 Frisch, M. J., Pople, J. A., & Binkley, J. S. 1984, *JCP*, 80, 3265
 Frisch, M. J., Trucks, G. W., Schlegel, H. B., et al. 2013, *Gaussian 09 Revision D.01* Wallingford CT
 Janson, M., Brandt, T. D., Kuzuhara, M., et al. 2013, *ApJL*, 778, L4
 Kreidberg, L., Beah, J. L., Desert, J. M., et al. 2014, *Natur*, 505, 69
 Line, M. R., Vasisht, G., Chen, P., Angerhausen, D., & Yung, Y. L. 2011, *ApJ*, 738, 32
 Mena, E. D., Israelian, G., Hernandez, J. I. G., et al. 2010, *ApJ*, 725, 2349
 Morley, C. V., Fortney, J. J., Kempton, E. M. R., et al. 2013, *ApJ*, 775, 33
 Moses, J. I., Visscher, C., Forthey, J. J., et al. 2011, *ApJ*, 737, 15
 Mousis, O., Luhine, J. I., Petit, J. M., et al. 2011, *ApJ*, 727, 77
 Negri, F., Castiglioni, C., Tommasini, M., & Zerbi, G. 2002, *JPCA*, 106, 3306
 Origlieri, M. 2014, ruff.info/R050503
 Perdew, J. P. 1986, *PhRvB*, 33, 8822
 Portmann, S., & Luthi, H. P. 2000, *Chimia*, 54, 766
 Pwa, T. H., Pottasch, S. R., & Mo, J. E. 1986, *A&A*, 164, 184

- Ricca, A., Bauschlicher, C. W., Boersma, C., Tielens, A. G. G. M., & Allamandola, L. J. 2012, *ApJ*, 754, 75
- Rimmer, P. B., Helling, C., & Bilger, C. 2014, *IJA*, 13, 173
- Russel, R. W., Soifer, B. T., & Willner, S. P. 1977, *ApJL*, 217, L149
- Russel, R. W., Soifer, B. T., & Willner, S. P. 1978, *ApJ*, 220, 568
- Sadezky, A., Muckenhuber, H., Grothe, H., Niessner, R., & Poschl, U. 2005, *Carbon*, 43, 1731
- Schindhelm, E., France, K., Herczeg, G. J., et al. 2012, *ApJL*, 756, 123
- Shafeev, G. A., Simakin, A. V., Lyalin, A. A., Obratsova, E. D., & Frolov, V. D. 1999, *ApSS*, 138, 461
- Simakin, A. V., Obratsova, E. D., & Shafeev, G. A. 2000, *CPL*, 332, 231
- Stephens, P. J., Devlin, F. J., Chabalowski, C. F., & Frisch, M. J. 1994, *JPC*, 98, 11623
- Stevenson, K. B., Harrington, J., Nymeyer, S., et al. 2010, *Natur*, 464, 1161
- Venot, O., Hebard, E., Angundez, M., et al. 2012, *A&A*, 546, A4
- Wieligor, M., Wang, Y. J., & Zerda, T. W. 2005, *JPCM*, 17, 2387
- Wilson, P. A., Colon, K. D., Sing, D. K., et al. 2014, *MNRAS*, 438, 2395
- Xie, W. J., & Wei, B. 2001, *ApPhL*, 79, 881
- Yurchenko, S. N., Tennyson, J., Bailey, J., Hollis, M. D. J., & Tinetti, G. 2014, *PNAS*, 111, 9379